Spin Waves in the Frustrated Kagomé Lattice Antiferromagnet $KFe_3(OH)_6(SO_4)_2$

K. Matan,[1] D. Grohol,[2] D. G. Nocera,[2] T. Yildirim,[3] A. B. Harris,[4] S. H. Lee,[3,5] S. E. Nagler,[6] and Y. S. Lee[1]

[1]*Department of Physics, Massachusetts Institute of Technology, Cambridge, Massachusetts 02139, USA*
[2]*Department of Chemistry, Massachusetts Institute of Technology, Cambridge, Massachusetts 02139, USA*
[3]*NIST Center for Neutron Research, Gaithersburg, Maryland 20899, USA*
[4]*Department of Physics and Astronomy, University of Pennsylvania, Philadelphia, Pennsylvania 19104, USA*
[5]*Department of Physics, University of Virginia, Charlottesville, Virginia 22904, USA*
[6]*Center for Neutron Scattering, Oak Ridge National Laboratory, Oak Ridge, Tennessee 37831, USA*

(Received 1 February 2006; published 19 June 2006)

The spin wave excitations of the $S = 5/2$ kagomé lattice antiferromagnet $KFe_3(OH)_6(SO_4)_2$ have been measured using high-resolution inelastic neutron scattering. We directly observe a flat mode which corresponds to a lifted ''zero energy mode,'' verifying a fundamental prediction for the kagomé lattice. A simple Heisenberg spin Hamiltonian provides an excellent fit to our spin wave data. The antisymmetric Dzyaloshinskii-Moriya interaction is the primary source of anisotropy and explains the low-temperature magnetization and spin structure.

DOI: 10.1103/PhysRevLett.96.247201 PACS numbers: 75.25.+z, 75.30.Ds, 75.50.Ee

Geometrically frustrated spin systems have received considerable attention in recent years due to the presence of remarkable properties such as spin ice [1,2], spin nematic [3], and spin-liquid behaviors [4–6]. The kagomé lattice antiferromagnet is a highly frustrated two-dimensional lattice, being comprised of corner-sharing triangles. For classical Heisenberg spins, the ground state of a kagomé antiferromagnet is infinitely degenerate, but the spins are believed to order in the $T \rightarrow 0$ limit by a process known as ''order by disorder'' [7,8]. On the other hand, there are predictions that the ground state of the $S = 1/2$ kagomé lattice is disordered, being a realization of the long sought after quantum spin liquid [4–6,9]. Experimentally, several materials have been studied that are believed to be realizations of the kagomé lattice antiferromagnet, such as SCGO [10,11], volborthite [12], and jarosites [13–15]. However, these materials are often plagued by nonstoichiometry issues or have structural differences from the ideal kagomé network. In this Letter, we present a high-resolution neutron scattering study on a pure single-crystal sample of the model kagomé antiferromagnet [16], iron jarosite $KFe_3(OH)_6(SO_4)_2$. This allows us to directly compare our data with fundamental theoretical predictions.

One of the hallmarks of highly frustrated systems is the presence of ''zero energy modes'' which result from the highly degenerate, but connected, ground-state manifold. For the kagomé lattice Heisenberg model, the only constraint for the ground state is that the spins on each triangle be oriented 120° relative to each other. A zero energy mode for the kagomé lattice is depicted in Fig. 1(a). The small loops at the tips of the spins illustrate rotations of two of the spin sublattices about the axis defined by the third spin sublattice. These spins, forming a chain, can collectively rotate around the loop paths with no change in energy (the 120° angles on each triangle are maintained). Furthermore, the spins on different parallel chains can be excited independently. Hence, this type of excitation costs no energy and is nondispersive [17]. This mode has not been directly observed previously, and since it occurs at zero energy, it is difficult to measure with most experimental techniques. Here we report in iron jarosite an observation of such a mode which is lifted to a finite energy due to the presence of spin anisotropy resulting from the Dzyaloshinskii-Moriya (DM) interaction [18,19].

$KFe_3(OH)_6(SO_4)_2$ is a very good realization of a kagomé Heisenberg antiferromagnet due to its undistorted lattice, fully occupied magnetic sites, and weak interlayer coupling [16,20]. The $S = 5/2$ Fe^{3+} ions form a kagomé arrangement and are surrounded by an octahedral environment of oxygens. Previous powder neutron diffraction studies [13,14] identified the long-range magnetic order below $T_N = 65$ K as that shown in Fig. 1(a). For this spin arrangement, each triangle has positive vector chirality [14,20], such that the spins rotate clockwise as one traverses the vertices of a triangle clockwise. Magnetization results on single crystals have determined that the spins are canted slightly out of the kagomé plane, yielding an ''umbrella'' structure. Moreover, each plane has a net ferromagnetic moment, with an antiferromagnetic coupling between adjacent planes [20].

We first studied the magnetic excitations using a deuterated powder sample (mass = 4.92 g) on the DCS and BT4 spectrometers at the NIST Center for Neutron Research, as shown in Figs. 1(b) and 1(c). For this sample, elemental analysis of the chemical composition and neutron powder refinement indicated that the K site occupancy was 100(1)%, the Fe site occupancy was >96%, and the level of deuteration was 100(1)%. Figure 1(c) shows a difference plot of the intensity as a function of neutron energy loss measured above ($T = 70$ K) and below ($T = 13$ K) the Néel temperature. This difference plot removes most of the phonon contributions to the spectrum, hence yielding the spin wave density of states. Despite the pow-

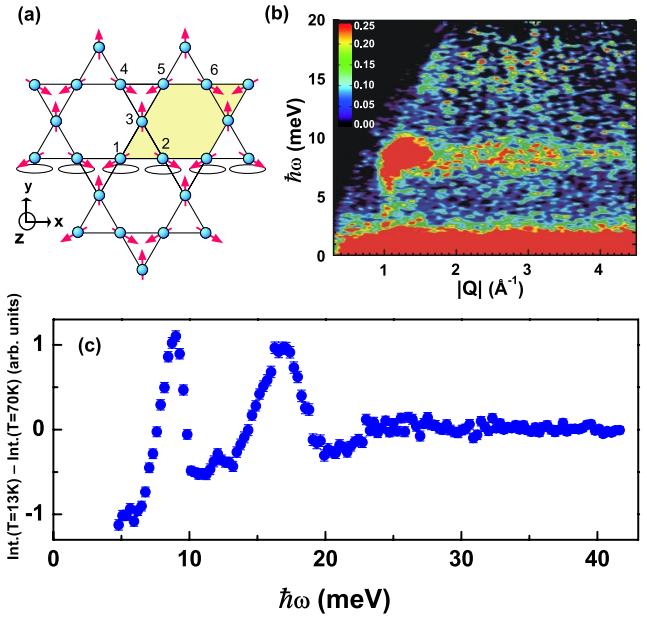

FIG. 1 (color online). (a) The ground-state spin configuration of iron jarosite. The magnetic unit cell, shown by the yellow shaded area, is the same as the chemical unit cell. The dotted loops illustrate the zero energy excitations as described in the text. The Cartesian axes and numbers are referred to in the discussion of the DM interaction. (b) Intensity contour map of the inelastic scattering spectrum at $T = 4$ K of a powder sample measured using the time-of-flight DCS spectrometer with an incident neutron wavelength of 1.8 Å. (c) Inelastic neutron scattering measured on a powder using the BT4 spectrometer with collimations 40′–20′. The data show the difference between the intensities above and below the Néel temperature $T_N = 65$ K and is a measure of the spin wave density of states.

der average, the spectrum shows one sharp feature at $\hbar\omega_0 \sim 8$ meV and a second broad peak at about $2\omega_0$. Both features appear as excitation bands over a wide range of $|\vec{Q}|$, as shown in Fig. 1(b). This behavior is quite similar to that observed in strongly frustrated spinel systems where the excitation at ω_0 has been described as a local resonance [21]. At first sight, it is tempting to identify the features observed in the excitation spectrum as one- and two-magnon scattering since strong multimagnon scattering might be expected due to the strong frustration and cubic terms in the spin Hamiltonian resulting from the noncollinear spin structure. However, as shown below, our single-crystal measurements provide much greater detail and demonstrate that these are regular spin wave modes, albeit with unusual dispersive behavior.

The spin wave dispersions were obtained from inelastic neutron scattering measurements on a nondeuterated single-crystal sample (composed of four coaligned crystals of total mass 101 mg) grown using a hydrothermal method reported previously [16,20]. High-resolution measurements were performed using the triple-axis spectrometer HB1 at the High Flux Isotope Reactor at Oak Ridge National Laboratory with the sample aligned in the (HK0) and (HHL) zones with the final energy fixed at either 13.6 or 14.7 meV. Vertically focused pyrolytic graphite (PG) crystals were used to monochromate and analyze the incident and scattered neutron beams using the (0 0 2) reflection. Horizontal collimations of 48′-60′-sample-40′-120′ were employed, and PG filters were placed in the scattered beam to reduce higher-order contamination. The sample was cooled to $T = 10$ K using a closed cycle ^{4}He cryostat.

A series of energy scans (at constant $\vec{Q}$) and $\vec{Q}$ scans (at constant energy) were performed, and a few representative scans are shown in Fig. 2. The observed peaks were initially fit with narrow Gaussians convoluted with the experimental resolution function. Subsequent fits were performed taking into account the empirical dispersion of the excitations. The peaks are resolution limited, and the line shapes are simply governed by the convolution with the instrumental resolution. A summary of all of the peak positions and intensities is shown in Fig. 3(a). The error bars plotted in Figs. 3(a) and 3(b) correspond to 3 times the statistical error or one-tenth of the instrumental resolution, whichever is larger. The most striking feature of the data is the relatively flat mode near 7 meV which barely disperses, even out to the zone boundary.

The energy scan in Fig. 2(a) at the magnetic Brillouin zone center (1 0 0) reveals two spin gaps, one at 1.8(1) meV (which is nondegenerate), and the other at 6.7(1) meV (which is twofold degenerate within the experimental resolution). At $\vec{Q} = (1.1\ 0\ 0)$ the lower-energy mode has dispersed to higher energy and merges with the flat mode located around 7 meV. The other upper-energy mode disperses strongly, moving to a high zone boundary energy of about 19 meV. Figure 2(c) shows constant-Q

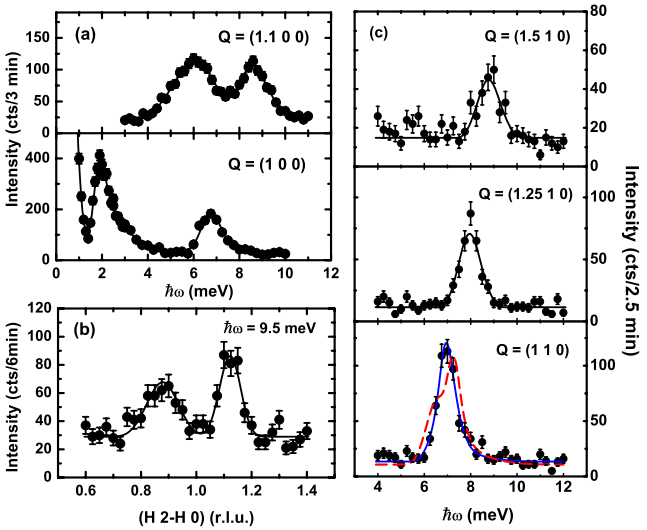

FIG. 2 (color online). (a) Energy scans at $\vec{Q} = (1\ 0\ 0)$ and (1.1 0 0) at $T = 10$ K. (b) $\vec{Q}$ scan at $\hbar\omega = 9.5$ meV. (c) Energy scans at $\vec{Q} = (1\ 1\ 0)$, (1.25 1 0), and (1.5 1 0). The solid lines show the fits to the spin wave dispersion relation described in the text, convoluted with the instrumental resolution function. In the lower panel of (c), the CF prediction is shown by the red dashed line and the DM prediction by the blue solid line.

scans of the flat mode within a Brillouin zone centered at (1 1 0). This excitation barely disperses, starting from about 7 meV at the zone center and reaching about 9 meV at the zone boundary. We identify this flat mode as the zero energy mode of the kagomé lattice which is lifted in energy for reasons discussed below.

We have fit the observed spin wave dispersions using the following generic Hamiltonian [22]:

$$\mathcal{H} = \sum_{\mathrm{nn}}[J_1\vec{S}_i\cdot\vec{S}_j + \vec{D}_{ij}\cdot\vec{S}_i\times\vec{S}_j] + \sum_{\mathrm{nnn}}J_2\vec{S}_k\cdot\vec{S}_l + D\sum_i(S_i^{y'})^2 - E\sum_i[(S_i^{z'})^2 - (S_i^{x'})^2], \quad (1)$$

where $\sum_{\mathrm{nn}}$ ($\sum_{\mathrm{nnn}}$) indicates summation over pairs of nearest neighbors (next-nearest neighbors), $\vec{D}_{ij} = [0, D_y(i,j), D_z(i,j)]$ is the DM vector for bond $i-j$ as shown in Fig. 1(a), and the single-ion anisotropy terms (D and E) are those used by Nishiyama *et al.* [23], where the primed spin components refer to the local axes associated with the rotated oxygen octahedra. We ignore the weak interplane coupling, which is several hundred times smaller than J_1 [20].

The DM interaction is allowed for this crystal structure and merits further discussion [24,25]. For bond 1–2 in Fig. 1(a), it has the form $\vec{D}_{1,2} = (0, D_y, D_z)$. The other DM vectors can be obtained from symmetry, such as $D_z(1,2) = D_z(2,3) = D_z(3,1)$, $D_y(4,5) = -D_y(1,2)$, and $D_z(4,5) = -D_z(1,2)$. Note that the direction of the DM vector oscillates from bond to bond along the x direction. The z component of the DM vector favors the spins to lie in the ab plane and therefore effectively acts like an easy-plane anisotropy. The sign of D_z breaks the symmetry between positive and negative vector chirality. The D_y component breaks the rotational symmetry around the c axis and creates an anisotropy with respect to in-plane orientations. The effect of D_y is also to cant the spins so that they have a small out-of-plane component, consistent with the observed umbrella spin configuration.

We may describe the spin wave data in terms of two simple spin models. In the first of these, which we call the DM model, we neglect the single-ion anisotropy, so that the only nonzero parameters are J_1, J_2, D_y, and D_z. In the second model, which we call the CF (crystal field) model, all the anisotropy is attributed to the single-ion crystal field, so that the only nonzero parameters are J_1, J_2, D, and E. In both cases, J_1 is the dominant interaction. The numerical results obtained from these two models are plotted as the lines in Fig. 3, and the approximate analytic expressions for the spin gaps at the Γ point are given in Table I.

To account for the observed umbrella spin structure, we considered the effect of spin canting on the spin wave energies. We find that the splitting of the mode energies at the high symmetry points are particularly sensitive to the magnitude of the spin-canting angle out of the kagomé plane. The best χ^2 fit to the DM model is depicted by the lines in Fig. 3(a) and describes the data very well. We reproduce not only the gaps at the zone center, but also the small dispersion of the flat mode. This small dispersion is a result of a weak nnn interaction J_2. We note that J_2 is positive, which favors the observed ground state. The D_z component of the DM vector also reinforces selection of this state. The zero energy mode is lifted by an energy equal to the out-of-plane spin wave gap, consistent with the spin rotations depicted in Fig. 1(a). The gaps at the Γ point obtained numerically are in good agreement with the analytic results given in Table I. The DM model yields a spin-canting angle of 1.9(2)°. This low-temperature value is

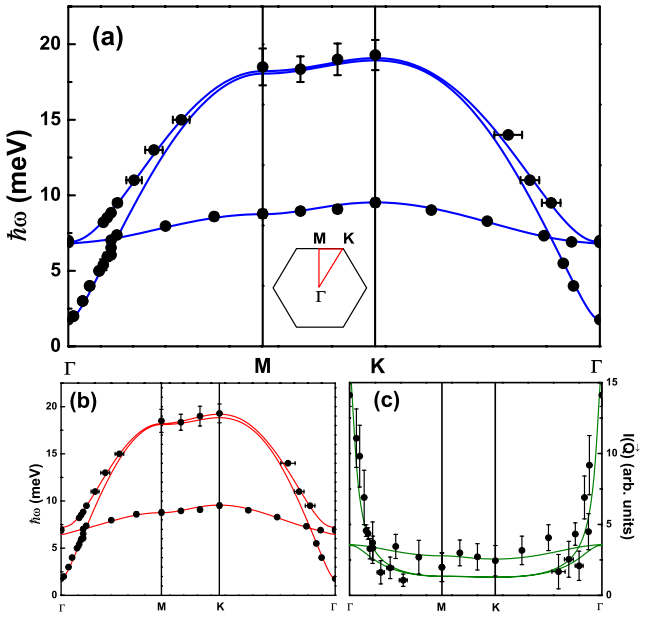

FIG. 3 (color online). Spin wave dispersion along the high symmetry directions in the 2D Brillouin zone at $T = 10$ K. As discussed in the text, the lines in (a) denote a fit to the DM model, with fit parameters $J_1 = 3.18(5)$, $J_2 = 0.11(1)$, $|D_y| = 0.197(2)$, and $D_z = -0.196(4)$ meV. The lines in (b) denote a fit to the CF model, with fit parameters $J_1 = 3.34(9)$, $J_2 = 0.12(2)$, $D = 0.428(5)$, and $E = 0.0316(3)$ meV. (c) Wave vector dependence of the spin wave intensities. The solid lines correspond to $[n(\omega)+1]/\omega(\vec{Q})$ with an overall scale factor as a fit parameter, where $n(\omega)$ is the Bose factor and $\omega(\vec{Q})$ is obtained from the DM model. The data take into account the deconvolution with the instrumental resolution and the Fe^{3+} magnetic form factor.

TABLE I. Spin wave energies at the zone center for the DM and CF models. Here, $\tilde{\omega} \equiv \omega/S$, $J \equiv J_1 + J_2$, $C_1 \equiv E - D\sin^2\theta_o + E\cos^2\theta_o$, $C_2 \equiv (D+E)\cos(2\theta_o)$, and $C_3 \equiv (D+E)\times \sin(2\theta_o)/2$, and $\theta_o \approx 20°$ is the oxygen octahedra tilting angle.

	DM model	CF model
$\tilde{\omega}_0$	$\sqrt{12}\lvert D_y\rvert$	$[12JC_1 + 4C_1C_2 + 4C_3^2]^{1/2}$
$\tilde{\omega}_\pm$	$[3D_y^2 + 18D_z^2 - 6\sqrt{3}JD_z]^{1/2}$ $\pm 2D_yD_z/J$	$[6JC_2 + 4C_1C_2 + 7C_3^2]^{1/2}$ $\pm C_3$

larger than the experimentally deduced canting angle of 0.65(6)° at $T = 50$ K [20], which is expected since the sublattice magnetization has not yet saturated at $T = 50$ K.

The lines in Fig. 3(b) show the best fit to the CF model, which also is in reasonable agreement with the data. However, the reduced-χ^2 value of 2.9 for the CF model fit is significantly higher than the reduced-χ^2 value of 0.63 for the DM model fit. The difference is most apparent in the numerical results for the mode splitting at the zone center. The CF model yields a relatively large splitting of about 0.71 meV for the 7 meV mode at the Γ point, whereas the data indicate that this splitting is smaller than 0.4 meV. The red dashed line in Fig. 2(c) shows the CF prediction for the energy scan at the zone center, and we see that this does not describe the line shape very well. The DM model, depicted by the blue solid line, describes the data better. Moreover, as pointed out in Ref. [24], the single-ion anisotropy of the Fe^{3+} ion is expected to be small since it appears at second order in the spin-orbit coupling, whereas the DM term appears at first order.

Therefore, we believe the observed spin wave spectrum is most naturally explained by a simple model which has only nearest and next-nearest isotropic interactions plus the DM interaction. The obtained fit parameters (in meV) are $J_1 = 3.18(5)$, $J_2 = 0.11(1)$, $|D_y| = 0.197(2)$, and $D_z = -0.196(4)$, where the error bars denote 3 times the statistical error. From a previous study [20], a value for J_1 of 3.9(2) meV was obtained from a fit of the susceptibility to a high-temperature series expansion result [17]. The values of J_1 are in reasonable agreement, and the agreement would be even closer if the effects of J_2 and the DM term were taken into account in the susceptibility fit. As a further comparison, the susceptibility in Ref. [20] indicated a value of $\Delta g/g \sim 0.06$, where g is the free electron Landé factor and Δg is its shift in the crystalline environment. The magnitude of the DM vector can be estimated from Moriya's calculation as $|\vec{D}|/J_1 \sim \Delta g/g$ [19]. From the current study, we have $D_y/J_1 \sim |D_z|/J_1 \sim 0.06 \sim \Delta g/g$, showing very good agreement between measurements of the spin dynamics and the bulk thermodynamics.

Finally, from the analytic expressions for the spin gaps given in Table I, we note that the in-plane gap is proportional to $|D_y|$, while the out-of-plane gaps are proportional to $\sqrt{J_1 D_z}$. Since J_1 is large compared to other interactions, the out-of-plane gap is significantly larger than the in-plane gap, despite the similar magnitude of D_y and D_z. This also suggests that at high temperatures (even above T_N), the spins would feel an easy-plane anisotropy and therefore display XY-like spin dynamics. This picture is consistent with the previous neutron scattering measurements of the critical fluctuations above T_N which indeed have XY symmetry [20]. That previous study also showed that uniform vector chiral order is apparent above T_N, consistent with the presence of the DM term and the positive sign of J_2.

In summary, the spin wave spectrum of a kagomé lattice antiferromagnet has been measured using inelastic neutron scattering. We observe a flat, lifted zero energy mode at ~7 meV, whose presence reflects the huge ground-state degeneracy of the ideal kagomé Heisenberg antiferromagnet. We have also determined the relevant spin-Hamiltonian parameters by fitting our data to a Heisenberg model with the antisymmetric DM interaction. This realization of the kagomé antiferromagnet is perhaps the best characterized geometrically frustrated spin system, and, as such, would be useful for precise tests of theoretical predictions. These results also highlight the importance of single-crystal measurements for accurate interpretation of data acquired with powder samples of frustrated magnets.

We thank M. D. Lumsden, J. W. Lynn, Q. Huang, and J. R. D. Copley for useful discussions. The work at MIT was supported by the NSF under Grant No. DMR 0239377, and in part by the MRSEC program under Grant No. DMR 02-13282. This work used facilities supported in part by the NSF under Agreement No. DMR-0454672. ORNL is managed for the U.S. DOE by UT-Battelle, LLC under Contract No. DE-AC05-00OR22725.

[1] A. P. Ramirez *et al.*, Nature (London) **399**, 333 (1999).
[2] J. Snyder *et al.*, Nature (London) **413**, 48 (2001).
[3] J. T. Chalker *et al.*, Phys. Rev. Lett. **68**, 855 (1992).
[4] C. Waldtmann *et al.*, Eur. Phys. J. B **2**, 501 (1998).
[5] S. Sachdev, Phys. Rev. B **45**, 12 377 (1992).
[6] C. Zeng and V. Elser, Phys. Rev. B **51**, 8318 (1995).
[7] D. A. Huse and A. D. Rutenberg, Phys. Rev. B **45**, 7536 (1992).
[8] J. N. Reimers and A. J. Berlinsky, Phys. Rev. B **48**, 9539 (1993).
[9] P. Sindzingre *et al.*, Phys. Rev. Lett. **84**, 2953 (2000).
[10] A. P. Ramirez, G. P. Espinosa, and A. S. Cooper, Phys. Rev. Lett. **64**, 2070 (1990).
[11] C. Broholm *et al.*, Phys. Rev. Lett. **65**, 3173 (1990).
[12] Z. Hiroi *et al.*, J. Phys. Soc. Jpn. **70**, 3377 (2001).
[13] A. S. Wills, Phys. Rev. B **63**, 064430 (2001).
[14] T. Inami *et al.*, Phys. Rev. B **61**, 12 181 (2000).
[15] S. H. Lee *et al.*, Phys. Rev. B **56**, 8091 (1997).
[16] D. Grohol *et al.*, Phys. Rev. B **67**, 064401 (2003).
[17] A. B. Harris, C. Kallin, and A. J. Berlinsky, Phys. Rev. B **45**, 2899 (1992).
[18] I. Dzyaloshinkii, J. Phys. Chem. Solids **4**, 241 (1958).
[19] T. Moriya, Phys. Rev. **120**, 91 (1960).
[20] D. Grohol *et al.*, Nat. Mater. **4**, 323 (2005).
[21] S. H. Lee *et al.*, Phys. Rev. Lett. **84**, 3718 (2000).
[22] T. Yildirim and A. B Harris, cond-mat/0603280 [Phys. Rev. B (to be published)].
[23] M. Nishiyama *et al.*, Phys. Rev. B **67**, 224435 (2003).
[24] M. Elhajal *et al.*, Phys. Rev. B **66**, 014422 (2002); R. Ballou *et al.*, J. Magn. Magn. Mater. **262**, 465 (2003).
[25] U. Bhaumik and A. Taraphder, cond-mat/0601612.